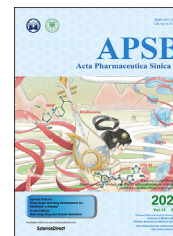




Chinese Pharmaceutical Association  
Institute of Materia Medica, Chinese Academy of Medical Sciences

Acta Pharmaceutica Sinica B

[www.elsevier.com/locate/apsb](http://www.elsevier.com/locate/apsb)  
[www.sciencedirect.com](http://www.sciencedirect.com)



ORIGINAL ARTICLE

# Inhibiting collagen I production and tumor cell colonization in the lung *via* miR-29a-3p loading of exosome-/liposome-based nanovesicles



Yan Yan<sup>a,b</sup>, Cancan Du<sup>a</sup>, Xixi Duan<sup>a</sup>, Xiaohan Yao<sup>a</sup>, Jiajia Wan<sup>a</sup>,  
Ziming Jiang<sup>c</sup>, Zhongyu Qin<sup>d</sup>, Wenqing Li<sup>a</sup>, Longze Pan<sup>a</sup>,  
Zhuoyu Gu<sup>a</sup>, Fazhan Wang<sup>a,\*</sup>, Ming Wang<sup>a,\*</sup>, Zhihai Qin<sup>a,b,e,\*</sup>

<sup>a</sup>Medical Research Center, the First Affiliated Hospital of Zhengzhou University, Zhengzhou University, Zhengzhou 450052, China

<sup>b</sup>Academy of Medical Sciences, Zhengzhou University, Zhengzhou 450052, China

<sup>c</sup>Department of Urology, the First Affiliated Hospital of Zhengzhou University, Zhengzhou University, Zhengzhou 450052, China

<sup>d</sup>Changzhi Medical College, Changzhi 046000, China

<sup>e</sup>Institute of Biophysics, Chinese Academy of Sciences, Beijing 100101, China

Received 14 April 2021; received in revised form 13 May 2021; accepted 2 June 2021

## KEY WORDS

Lung metastasis;  
miR-29a-3p;  
Collagen I;  
Liposomal nanovesicle;  
Exosomes;  
Fibroblasts;  
Pre-metastatic niche

**Abstract** The lung is one of the most common sites for cancer metastasis. Collagens in the lung provide a permissive microenvironment that supports the colonization and outgrowth of disseminated tumor cells. Therefore, down-regulating the production of collagens may contribute to the inhibition of lung metastasis. It has been suggested that miR-29 exhibits effective anti-fibrotic activity by negatively regulating the expression of collagens. Indeed, our clinical lung tumor data shows that miR-29a-3p expression negatively correlates with collagen I expression in lung tumors and positively correlates with patients' outcomes. However, suitable carriers need to be selected to deliver this therapeutic miRNA to the lungs. In this study, we found that the chemotherapy drug cisplatin facilitated miR-29a-3p accumulation in the exosomes of lung tumor cells, and this type of exosomes exhibited a specific lung-targeting effect and promising collagen down-regulation. To scale up the preparation and simplify the delivery system, we designed a lung-targeting liposomal nanovesicle (by adjusting the molar ratio of DOTAP/cholesterol

**Abbreviations:** cDNA, complementary DNA; CPT-Exo, cisplatin elicited lung tumor exosomes; CTCs, circulating tumor cells; DOTAP, 1,2-dioleoyl-3-trimethylammonium propane; ECM, extra cellular matrix; EVs, extracellular vesicles; LLC, Lewis lung carcinoma; LLC-Exo, LLC-derived exosomes; Luc-LPX, Luc-lipoplex; miR-29a-3p-LPX, miR-29a-3p-lipoplex; NC inhibitor, negative control inhibitor; NC mimic, negative control mimic; PMN, pre-metastatic niche; RNA-LPX, RNA-lipoplex.

\*Corresponding authors. Tel./fax: +86 371 66913632.

E-mail addresses: [fazhanwang\\_20@zzu.edu.cn](mailto:fazhanwang_20@zzu.edu.cn) (Fazhan Wang), [wangmingheda@163.com](mailto:wangmingheda@163.com) (Ming Wang), [zhihai@ibp.ac.cn](mailto:zhihai@ibp.ac.cn) (Zhihai Qin).

<https://doi.org/10.1016/j.apsb.2021.08.011>

2211-3835 © 2022 Chinese Pharmaceutical Association and Institute of Materia Medica, Chinese Academy of Medical Sciences. Production and hosting by Elsevier B.V. This is an open access article under the CC BY-NC-ND license (<http://creativecommons.org/licenses/by-nc-nd/4.0/>).

–miRNAs to 4:1) to carry miR-29a-3p and mimic the exosomes. This liposomal nanovesicle delivery system significantly down-regulated collagen I secretion by lung fibroblasts *in vivo*, thus alleviating the establishment of a pro-metastatic environment for circulating lung tumor cells.

© 2022 Chinese Pharmaceutical Association and Institute of Materia Medica, Chinese Academy of Medical Sciences. Production and hosting by Elsevier B.V. This is an open access article under the CC BY-NC-ND license (<http://creativecommons.org/licenses/by-nc-nd/4.0/>).

## 1. Introduction

Tumor metastasis is a critical phase of cancer progression and is the major cause of tumor-related mortality, accounting for approximately 90% of tumor-related deaths<sup>1</sup>. It is widely accepted that metastasis is a complex multistep process<sup>2</sup>. Metastatic tumor cells detach from primary tumor sites, travel into circulating or lymphatic vessels, and extravasate and seed into secondary sites. Metastatic cells can encourage the formation of macro-metastases by establishing an amenable microenvironment for metastasis through manipulation of the microenvironment<sup>3</sup>. The lungs are one of the most frequent sites of metastasis in both preclinical models and cancer patients, and almost all cancers have the capacity to spread to the lungs<sup>4</sup>. It is believed that the specific lung tumor microenvironment, including the extracellular matrix (ECM), vasculature, cancer-associated fibroblasts, and degree of infiltration of immune cells, play a major role in tumor metastases<sup>5</sup>.

Increased collagen expression or deposition is correlated with poor prognosis in lung cancer patients<sup>6,7</sup>. In lung tissue, type I collagen is the most abundant subtype and ECM protein produced by lung fibroblasts<sup>8</sup>. Collagen I can promote epithelial–mesenchymal transition (EMT) by enhancing Snail stability<sup>9</sup>, and type I collagen in lung cancer accelerates tumor cell growth and metastasis<sup>10</sup>, though targeting collagen I therapeutically has been challenging<sup>11</sup>.

miRNAs are small non-coding RNAs that act as epigenetic regulators by silencing a broad set of target genes and affecting various processes in tumor development<sup>12</sup>. The effects of miRNAs on collagen expression have been investigated<sup>13</sup>. miR-29 exhibits strong anti-fibrotic activity by negatively regulating collagens and thus inhibits the progress of fibrotic skin diseases and systemic sclerosis<sup>14</sup>. In tumors, miR-29 knockdown increased the ability of ovarian cancer cells to escape cisplatin-induced cell death *via* up-regulating collagen I<sup>15</sup>. Therefore, overexpression of miR-29 may have therapeutic potential for lung tumor metastasis treatment. However, the therapeutic efficacy of miR-29 on inhibiting collagens expression and tumor cell metastasis in the lung has not been investigated. Moreover, another challenge in the current study is how to maintain the stability of target miRNAs during delivery *in vivo* since miRNAs are quickly degraded and cleared in the blood circulation.

Exosomes, widely recognized natural nanovesicles, are membrane-bound extracellular vesicles (EVs) produced in the endosomal compartment of eukaryotic cells<sup>16</sup>. Based on their biological compatibility and particularly small size, exosomes have recently been investigated as suitable substitutes for the shortcomings of nanoparticles<sup>17</sup>. Moreover, it has been documented that exosomes play vital roles in cell communication by delivering biological cargoes, including miRNAs, throughout the body<sup>18</sup>. Apart from exosomes, therapeutic miRNA-enriched liposomes can also be used for disease treatment by targeting pathological recipient cells<sup>19</sup>. However, there are limitations and

gaps in our knowledge in how to enrich the target miRNAs in naturally produced exosomes and how to specifically transport nanovesicles to target organs. Here, we report that cisplatin treatment significantly enhances the miR-29a-3p concentration in lung tumor exosomes. We have also developed a liposome-based nano-delivery system, miR-29a-3p-lipoplex (miR-29a-3p-LPX), to inhibit collagen expression in the lung. Overall, cisplatin elicited exosomes (CPT-Exo), and miR-29a-3p-LPX represent a promising strategy for lung tumor metastasis treatment.

## 2. Materials and methods

### 2.1. Cell models

The mouse Lewis lung carcinoma (LLC) cell line was kindly gifted by Professor Li Yan (Academy of Military Medical Sciences, Beijing, China). The immortalized mouse embryonic fibroblast (iMEF) cell line was a gift from Professor Lin Xi (Tsinghua University, Beijing, China). The human normal lung fibroblast cell line CCD-19Lu was purchased from ATCC (ATCC CCL-210). Stable enhanced green fluorescent protein (EGFP) and luciferase-expressing LLC cells (LLC-EGFP-Luc) used for bioluminescent tracking were generated by lentiviral infection per the manufacturer's instructions; the lentivirus particles containing the Ubi-MCS-EGFP-SV40-firefly\_Luciferase-IRES-Puromycin vector were purchased from GeneChem (Shanghai, China). EGFP positive clones were selected by FACS. All cells were cultured in Dulbecco's modified Eagle's medium (DMEM; HyClone, Logan, UT, USA) supplemented with 10% FBS (PAN Biotech, Aidenbach, Germany), 100 IU/mL penicillin and 100 µg/mL streptomycin (Gibco, Waltham, MA, USA) at 37 °C in a 5% CO<sub>2</sub> incubator.

### 2.2. Isolation of mouse lung fibroblasts

Primary mouse lung fibroblasts were isolated from the lungs of one-week-old C57BL/6N mice per previously published methods<sup>20</sup>. Briefly, lung tissues were collected aseptically and flushed with PBS to remove excess blood contamination and then minced into 1- to 2-mm pieces in FBS. The minced lungs were placed in culture flasks for 2 h and cultured in DMEM. After 5–7 days of proliferation, fibroblasts were used for *in vitro* experiments.

### 2.3. RNA interference

Mouse lung fibroblasts, iMEF cells, and CCD-19Lu cells were transfected with 50 nmol/L of mouse or human miR-29a-3p mimic, negative control mimic (NC mimic), antisense miR-29a-3p inhibitor or negative control inhibitor (NC inhibitor), using Lipofectamine RNAiMax (13778030, Invitrogen, Waltham, MA, USA) per the manufacturer's instructions. miR-29a-3p mimic, miR-29a-3p inhibitor, and their corresponding negative controls

were purchased from Sangon Biotech (Shanghai, China). The sequences are listed in Supporting Information [Tables S1 and S2](#).

#### 2.4. Dual-luciferase reporter assay

The *Coll1a1* 3' UTR luciferase reporter plasmid for miR-29a-3p was commercially constructed (GeneChem, Shanghai, China). The murine *Coll1a1* 3' UTR sequence containing a wild-type (WT: TGGTGCT) or mutated miR-29a-3p (Mut: GTTGAG) binding site was subcloned into the pMIR-reporter firefly luciferase vector (SV40-firefly\_Luciferase-MCS) via the XbaI/XbaI sites. HEK293T cells were transfected with wild-type or mutant *Coll1a1* 3' UTR-luciferase reporter plasmid together with Renilla luciferase plasmid (TK promoter-Renilla\_luciferase) as a control reporter vector, using Lipofectamine 3000 reagent (Invitrogen, Waltham, MA, USA). miR-29a-3p mimic or NC mimic was transfected using Lipofectamine RNAiMax (L3000015, Invitrogen, Waltham, MA, USA) simultaneously. Luciferase activity was measured 24 h post-transfection using the Dual-Luciferase Reporter Gene Assay Kit (Beyotime, Shanghai, China) on a microplate reader (SpectraMax i3x, Molecular Devices, Sunnyvale, CA, USA). The relative luciferase activity in miR-29a-3p mimic transfected cells was determined by calculating the ratio of firefly to co-transfected Renilla luciferase activity and comparing it with NC mimic transfected cells.

#### 2.5. Bioluminescence imaging

LLC-EGFP-Luc metastatic tumors were evaluated by bioluminescence imaging using the Xenogen IVIS Spectrum imaging system (Caliper Life Sciences, Hopkinton, MA, USA). Intraperitoneal injection of D-luciferin was performed (150 mg luciferin/kg body weight) 10 min before imaging. Mice were anesthetized with 2% isoflurane by inhalation. Whole-body and mice lung imaging were performed.

#### 2.6. Western blotting

Cells, exosomes, or tissues were lysed on ice in radioimmunoprecipitation assay buffer supplemented with 1% protease inhibitor cocktail (P8340, Sigma-Aldrich, St. Louis, MO, USA) and 1 mmol/L phenylmethylsulfonyl fluoride for 30 min. Protein concentrations were determined using the Pierce BCA Protein Assay Kit (232225, Thermo Scientific, Rockford, IL, USA) per the manufacturer's instructions. Next, 20 µg of total protein was separated by SDS-PAGE on a 10% gel and transferred electrophoretically to a nitrocellulose filter membrane (HATF00010, Millipore, Billerica, MA, USA). Fast green FCF staining of the nitrocellulose membranes after transfer confirmed equal protein loading. The details of the antibodies used are provided in Supporting Information [Table S3](#).

#### 2.7. RNA isolation and quantitative real-time RT-PCR

Total mRNA was isolated from cells with RNAiso Plus (9109, Takara, Tokyo, Japan), and complementary DNA (cDNA) was synthesized using the PrimeScript RT Master Mix (RR036A; Takara, Tokyo, Japan). For quantitative miRNA analysis, total RNA was extracted from exosomes or cells using the miRNeasy Mini Kit (217004, Qiagen, Hilden, Germany). Reverse transcription was conducted with a miRNA First Strand cDNA Synthesis (Stem-loop Method) Kit (B532453, Sangon Biotech,

Shanghai, China). cDNA was quantified by real-time PCR using TB Green Premix Ex Taq II (RR820A, Takara, Tokyo, Japan) on an ABI PRISM 7300HT Sequence Detection 542 System (Applied Biosystems, Foster City, CA, USA). The primer sequences are listed in Supporting Information [Table S4](#). Relative expression of each gene was normalized with GAPDH for RNA and U6 for miRNA.

#### 2.8. Exosome isolation and identification

LLC-derived exosomes (LLC-Exo) and CPT-Exo were isolated from culture supernatants by multi-step centrifugation as previously described<sup>21</sup>. Briefly, 80% confluent cells were rinsed with PBS and then cultured in FBS-free DMEM with 5 µmol/L cisplatin (or control vehicle PBS). After 24 h, the culture medium was collected and centrifuged at 200×g for 10 min and 20,000×g for 20 min at 4 °C to remove dead cells and debris. The supernatant was then subjected to ultracentrifugation at 100,000×g for 70 min at 4 °C on a HITACHI ultracentrifuge (CS150FNX, Tokyo, Japan). The obtained exosome pellet was washed with PBS and concentrated after ultracentrifugation. The purification of exosomes was verified by transmission electron microscopy (HT7800, HITACHI, Tokyo, Japan) and the expression of exosome-specific markers CD63 and HSP90 by western blotting.

#### 2.9. Exosome treatment

Exosomes were suspended in PBS and filtered through 0.22 µm filters before use. For the exosome *in vitro* treatment, fibroblasts were seeded at  $2 \times 10^4$  cells per well in 12-well plates and cultured in serum-free medium. After overnight culture, exosomes were added in medium to a final concentration of 50 µg/mL. Cells were harvested 3 h post-treatment for RNA extraction and 24 h post-treatment for protein extraction. For *in vivo* exosome treatment, each mouse (Female C57BL/6N, wild-type, 6–8-week-old, Charles River Laboratories, Beijing, China) was injected with 100 µL of exosome solution via the tail vein at a dose of 0.5 mg/kg body weight. The treatment was given every three days for a total of three times. Mice were sacrificed for lung harvest three days after the last treatment or injected with  $5 \times 10^5$  LLC-EGFP-Luc cells per mouse to analyze the incidence of metastasis.

#### 2.10. RNA-sequencing

To identify the gene expression profile of lung fibroblasts stimulated with LLC-Exo/CPT-Exo, RNA sequencing was performed by OE Biotech Co., Ltd. (Shanghai, China) using the Illumina HiSeq 2500 (Illumina, San Diego, CA, USA). Lung fibroblasts were treated with 50 µg/mL exosomes, incubated for 3 h then collected for RNA sequencing. The data were analyzed using EdgeR software, and statistical significance for differential gene expression was defined as  $P < 0.05$ . RNA sequencing data were uploaded to the Sequence Read Archive (SRA) database with the accession numbers SRR13079646 and SRR13079645.

#### 2.11. Microarray analysis

To analyze the difference in miRNAs loaded into LLC-Exo and CPT-Exo, microarray analysis using Mouse miRNA Microarray Kit, Release 21.0, 8 × 60 K (design ID: 070155; Agilent Technologies, Santa Clara, CA, USA) was performed at OE Biotech Co., Ltd. Labeling of miRNAs, microarray hybridization, and

washing were carried out based on the manufacturer's protocols. Data extraction and visualization were performed using Feature Extraction Software (Version 10.7.1.1; Agilent Technologies, Santa Clara, CA, USA). Primary data are available at the NCBI's Gene Expression Omnibus database (GSE142584 and GSE161832).

### 2.12. Cell adhesion assay

Lung fibroblasts were cultured until 95%–100% confluence after transfection in a 6-well plate, then LLC-mCherry cells were seeded into the culture system at  $2.0 \times 10^5$  cells per well. The plate was left undisturbed for 15 min in a humidified incubator at 37 °C with 5% CO<sub>2</sub>. Subsequently, nonadherent LLC-mCherry cells were removed by washing three times with PBS. Adhered cells were captured by using the Incucyte ZOOM System (Essen BioScience, Ann Arbor, MI, USA).

### 2.13. Soft agar colony formation assay

The colony-forming ability of LLC cells was evaluated using a soft agar colony formation assay. To form the lower layer, 1 mL of complete medium containing 0.6% low melting point agarose was added into a 6-well plate. After the agarose solidified, LLC cells were suspended at a density of  $1 \times 10^4$  cells per well with a top layer of complete medium containing 0.35% agarose. To examine the effect of lung fibroblasts transfected with miR-29a-3p mimic/inhibitor on the colony formation of LLC cells, conditioned medium was added every other day to the upper agar layer. Plates were incubated for 14 days at 37 °C in 5% CO<sub>2</sub> and colonies consisting of more than 50 cells were counted under the microscope.

### 2.14. Three-dimensional (3D) tumor spheroid invasion assay

Cell migration and invasion abilities were evaluated by a 3D Tumor Spheroid Invasion Assay as previously described<sup>22</sup>. The bottom of a 96-well plate was first coated with 80 µL of 1.5% low melting agarose to provide a low attachment U-bottom, and 5000 LLC cells were seeded per well in full serum medium after agarose solidification. Cells were cultured in a 37 °C, 5% CO<sub>2</sub> humidified incubator for four days until visible tumor spheroids formed. Ice-cold Matrigel mixed with lung fibroblast conditioned media was prepared at a final concentration of 2.5 mg/mL and placed in a 96-well plate ( $n = 3$  per condition and 100 µL volume per well), and collagen I (354236, Corning, NY, USA) was added at a final concentration of 2.5 mg/mL into the DMEM mixed Matrigel as a positive control. The blank DMEM mixed Matrigel acted as a negative control. The tumor spheroid was transferred carefully into the center position of mixed Matrigel using ice-cold pipette tips, and invasion of the spheroids was analyzed after 24 h in culture. Images were taken using a Leica inverted microscope. LLC cell proliferation was measured by Ki-67 staining and flow cytometry analysis.

### 2.15. Liposomes and miR-29a-3p-LPX preparation and characterization

miR-29a-3p-LPX was designed to deliver miR-29a-3p into the lung tissue of mice stably and efficiently. Cationic liposomes composed of 1,2-dioleoyl-3-trimethylammonium propane (DOTAP) and cholesterol (AVT Pharmaceutical Tech Co., Ltd.,

Shanghai, China) at molar proportions of 1:1 were produced based on the thin-film hydration method, forming colloiddally stable liposomes and then used to complex miR-29a-3p for the formation of colloiddally stable miR-29a-3p-LPX by a simple self-assembly method<sup>23</sup>. The miRNA was specifically delivered to the lung by adjusting the ratio of lipid to RNA (positive to negative charge ratio) to 4:1<sup>19</sup>. Reporter firefly luciferase encoding RNA was assembled with liposomes to form Luc-lipoplex (Luc-LPX), which was used to evaluate the lung targeting specificity of RNA-lipoplex (RNA-LPX) *in vivo* by bioluminescence imaging. miR-29a-3p-LPX and miR-29a-3p-LPX negative control (NC-LPX) were formed by diluting the RNA with RNase-free H<sub>2</sub>O and 9% NaCl solution and then incubated for 30 min at room temperature before tail vein injection. The size and morphology of miR-29a-3p-LPX were assayed by Malvern Zetasizer Version 7.04 and transmission electron microscopy, respectively.

### 2.16. LPX safety investigation

The safety of NC-LPX and miR-29a-3p-LPX were evaluated *in vitro* according to a previous study<sup>24</sup>. Briefly, 0.5 mL of LPX or other formulations were diluted in 2 mL with normal saline, then mixed with rabbit red blood cell suspension (2.5 mL) in glass tubes. Normal saline and distilled water were used as the negative and positive controls, respectively. The red blood cell suspension was centrifuged for 15 min at 300×g, then placed at 37 °C for 3 h. The hemolytic activity of LPX was recorded with a digital camera. The absorbances (Abs) of the supernatants of red blood cells treated with LPXs were measured at 545 nm. Finally, the percent of hemolysis of LPXs was calculated according to the following Eq. (1):

$$\text{Hemolysis (\%)} = (\text{Ab of LPXs} - \text{Ab of negative control}) / (\text{Ab of positive control} - \text{Ab of negative control}) \times 100 \quad (1)$$

### 2.17. Animal experiments

To examine the effect of miR-29a-3p on lung metastasis, a total volume of 200 µL per 20 g body weight of miR-29a-3p-LPX or NC-LPX containing 5 µg miR-29a-3p mimic or NC mimic was injected into mice every three days *via* the tail vein. Three days after miR-29a-3p-LPX pre-treatment,  $5 \times 10^5$  LLC-EGFP-Luc cells per mouse were intravenously injected. Mice were sacrificed 21 days after LLC-EGFP-Luc injection, and lung metastasis was measured by bioluminescence imaging and HE staining. All animal experiments were performed according to previous publications<sup>25</sup>. All protocols were approved by the Ethics Committee of Zhengzhou University (Ethical Approval Number: 2021-KY-0028). Briefly,  $5 \times 10^5$  LLC-EGFP-Luc cells were injected into mice *via* the tail vein after three rounds of miR-29a-3p-LPX and NC-LPX treatment. At 72 h post-LLC-EGFP-Luc injection, equal volumes (200 µL) of whole peripheral blood and lung tissue were collected simultaneously from euthanized mice. The frequency of circulating tumor cells (CTCs) in blood and infiltrated LLC tumor cells in lung tissue was examined by flow cytometry analysis. Lungs were dissociated into single-cell suspensions and prepared for flow cytometry (BD FACSCanto II) analysis. Data were analyzed using FlowJo (V10) software. All experiments were carried out on wild-type 6–8 weeks old C57BL/6N mice (Charles River Laboratories, Beijing, China).

### 2.18. Human lung cancer tissue cDNA microarrays

The human lung cancer tissue cDNA microarrays contained 15 pairs of lung adenocarcinoma cancer samples and matched adjacent normal tissue samples (Shanghai Outdo Biotech Co., Ltd., Shanghai, China). *COL1A1* expression was quantified by RT-PCR, and miR-29a-3p expression was determined using miRcute Plus miRNA qPCR Detection Kit (FP411; Tiangen Biotech, Beijing, China).

### 2.19. Statistical analysis

Statistical analysis was performed using GraphPad Prism8 software. Data were represented as mean  $\pm$  standard deviation (SD). Comparisons between two groups were made using paired or unpaired Welch's *t*-test as appropriate. For multiple comparisons, one-way or two-way ANOVA was applied as appropriate. Linear correlation was evaluated by the Pearson correlation coefficient (*r*). *P* values < 0.05 were considered statistically significant.

## 3. Results

### 3.1. miR-29a-3p down-regulates collagen I expression in lung fibroblasts

The anti-fibrotic function of miR-29 has been previously investigated<sup>26,27</sup>. To further confirm the inhibition of collagen I expression by miR-29 in the lung, we first used the online miRNA-mRNA matching tool TargetScan and identified that miR-29a-3p has the potential to target *Coll1a1* mRNA sites (Fig. 1A). Previous studies have suggested that lung fibroblasts are the main source of collagen I in lung tissue<sup>6,8</sup>. Therefore, we next investigated the mRNA expression of *Coll1a1* in different lung cell types, including primary isolated fibroblasts, CD45<sup>+</sup> immune cells, CD326<sup>+</sup> epithelial cells, CD31<sup>+</sup> endothelial cells, and other cells

(CD31<sup>-</sup>, CD326<sup>-</sup>, CD45<sup>-</sup>), and confirmed that lung fibroblasts are the major cell type for collagen I production (Supporting Information Fig. S1). In addition, we transfected miR-29a-3p mimics into primary lung fibroblasts and analyzed collagen I expression; transfection efficiency was identified by green fluorescence and found to be greater than 80% (Supporting Information Fig. S2). We observed a significant down-regulation of *Coll1a1* mRNA expression and collagen I secretion in miR-29a-3p transfected fibroblasts (Fig. 1B and C). Collagen I targeting by miR-29a-3p was substantiated by dual-luciferase reporter experiments (Fig. 1D and E). All these data confirm that miR-29a-3p has the potential to inhibit collagen I expression.

### 3.2. CPT-Exo contains a high level of miR-29a-3p and inhibits collagen I production

We next investigated the source of miR-29a-3p in different cell types. Compared with normal lung cell types, we found that lung tumor cell line LLC expressed a significantly high level of miR-29a-3p (Fig. 2A). However, our previous study showed that LLC-derived exosomes promoted LLC colonization in the lung<sup>25</sup>. So, LLC-Exo are not an appropriate carrier to deliver miR-29a-3p. Chemotherapy can induce a massive release of exosomes. Therefore, we further stimulated LLC cells with cisplatin (5  $\mu$ mol/L; 24 h) and collected exosomes from the culture supernatant. The purification of exosomes was verified by specific surface markers CD63/HSP90 and electronic microscopy (Fig. 2B and C). Interestingly, we observed that not only the total amount but also the relative concentration of miR-29a-3p in CPT-Exo increases approximately 4-fold (Fig. 2D). Moreover, cisplatin treatment induced 2.1 times up-regulation of circulating exosomal miR-29a-3p *in vivo* (Supporting Information Fig. S3). To examine the potential function of CPT-Exo in fibroblast gene profiles, RNA-seq was used to identify any modification to mRNA expression in lung fibroblasts stimulated with LLC-Exo or CPT-

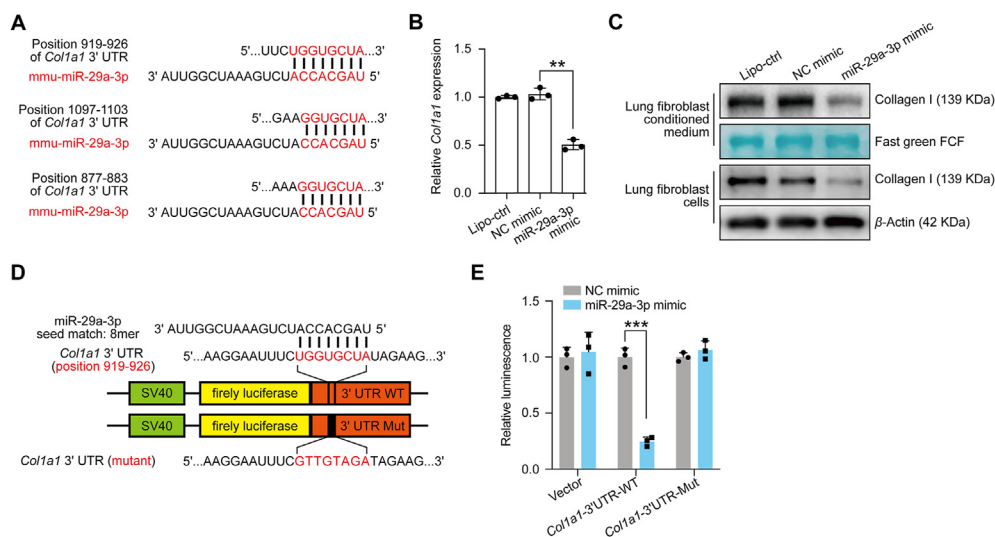


**Figure 1** miR-29a-3p targets *Coll1a1* in lung fibroblasts. (A) miR-29a-3p binding sites in the *Coll1a1* mRNA 3' UTR, predicted using TargetScan. (B) and (C) Lung fibroblasts transfected with blank liposome, NC mimic, or miR-29a-3p mimic. Relative *Coll1a1* mRNA and protein levels were analyzed by qRT-PCR and Western blotting ( $n = 3$ ; mean  $\pm$  SD; One-way ANOVA). Post-transcriptional regulation of *Coll1a1* by miR-29a-3p analyzed *via* dual-luciferase reporter assay. (D) The wild type (WT) and mutated (Mut) reporter constructs of the *Coll1a1* 3' UTR sequence are shown in the schematic diagram. (E) Relative luciferase activity was normalized to the Renilla luciferase activity and calculated compared with NC mimic transfected cells ( $n = 3$ ; mean fold changes  $\pm$  SD; multiple *t*-test). \*\* $P < 0.01$ , \*\*\* $P < 0.001$ .

Exo. Among the altered genes in CPT-Exo-treated fibroblasts, *Coll1a1* was the most significantly down-regulated by CPT-Exo (Supporting Information Fig. S4). The powerful collagen I inhibition effect of CPT-Exo was also confirmed by mRNA and protein levels. The CPT-Exo treatment caused stronger inhibition of collagen I expression in both primary lung fibroblasts and the fibroblast cell line iMEF (Fig. 2E and F). Intravascularly injected CPT-Exo also decreased the total protein concentration of collagen I in the lungs (Fig. 2G and H), which was further confirmed by Masson and immunohistochemical staining (Fig. 2I and J). In addition, we also examined the entry effect of LLC-Exo and CPT-Exo and found that the potential uptake of these

exosomes by lung fibroblasts was similar *in vitro* and *in vivo* (Supporting Information Fig. S5).

To further investigate the specificity of exosomal miR-29a-3p in the inhibition of collagen I expression, we first confirmed the dose-dependent collagen I inhibition of miR-29a-3p mimic on fibroblasts (Supporting Information Fig. S6). Next, we treated lung fibroblasts with CPT-Exo combined with miR-29a-3p antagonist and found the miR-29a-3p antagonist could reverse collagen I down-regulation in both cell lysate and supernatant (Fig. 2K and L). Collagen I secretion in both mouse and human fibroblast cell lines iMEF and CCD19 was inhibited by the miR-29a-3p mimic; on the contrary, CPT-Exo impaired collagen I

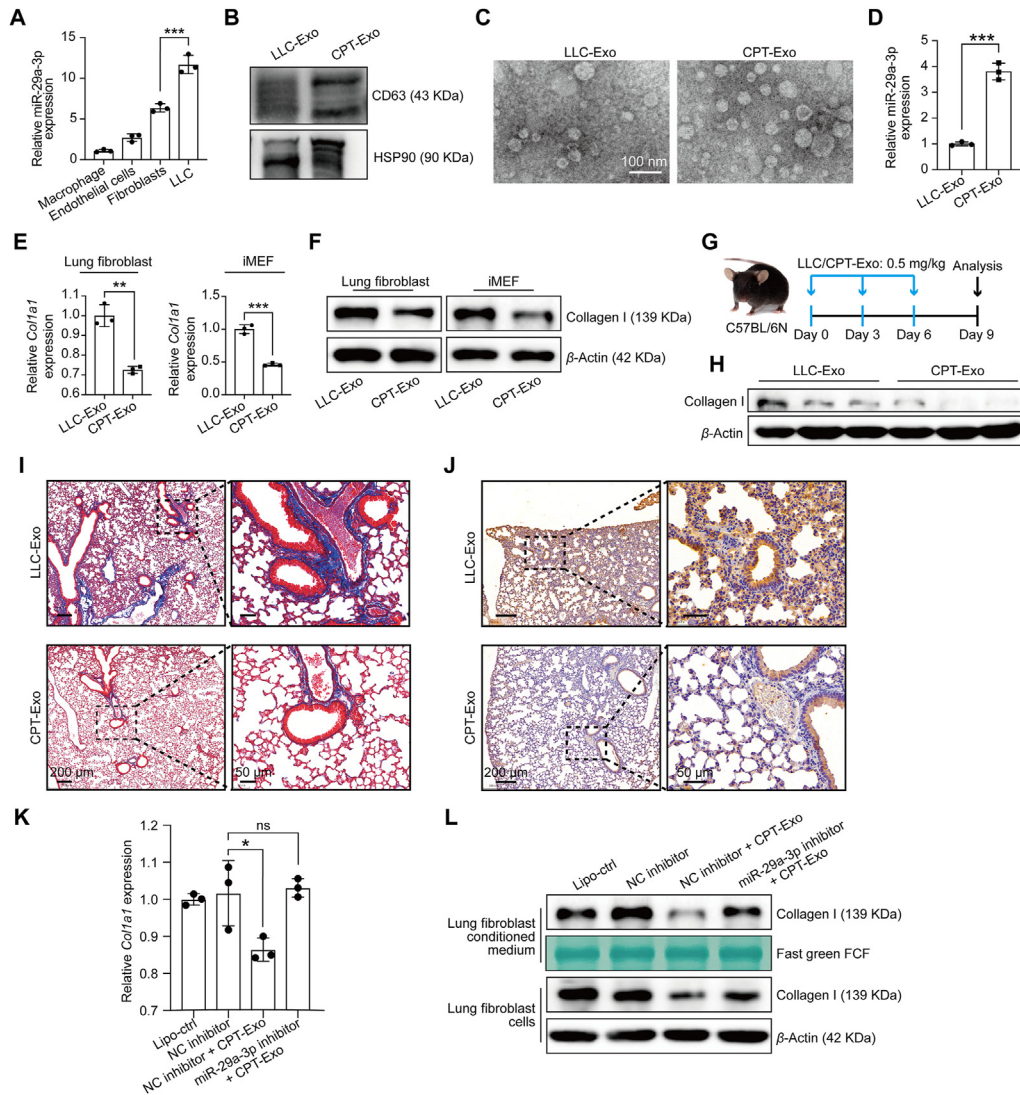


**Figure 2** miR-29a-3p loading into CPT-Exo down-regulated collagen I expression in lung fibroblasts. (A) Relative miR-29a-3p expression levels in different cell types analyzed by qRT-PCR ( $n = 3$ ; mean  $\pm$  SD; One-way ANOVA). (B) Representative Western blots showing the expression of exosome markers CD63 and HSP90. (C) Representative TEM photograph of LLC-Exo and CPT-Exo. Scale bar = 100 nm. (D) miR-29a-3p expression levels in LLC-Exo and CPT-Exo, analyzed by qRT-PCR ( $n = 3$ ; mean  $\pm$  SD; Welch's  $t$ -test). Mouse lung fibroblasts and iMEFs treated with LLC-Exo or CPT-Exo. (E) *Coll1a1* expression levels determined by qRT-PCR ( $n = 3$ ; mean  $\pm$  SD; Welch's  $t$ -test). (F) Collagen I protein levels detected by Western blotting. (G) Schematic illustrating the exosome treatment assays. (H) After three exosome injections, the lungs were collected, and the collagen levels were detected by Western blotting. Masson staining (I), immunohistochemical analysis (J). Representative images are shown. Scale bar = 200  $\mu$ m (left) and 50  $\mu$ m (right). Relative *Coll1a1* mRNA (K) and collagen I protein (L) levels in mouse lung fibroblasts transfected with blank liposome, NC inhibitor, or miR-29a-3p inhibitor with or without CPT-Exo stimulation, analyzed by qRT-PCR and Western blotting ( $n = 3$ ; mean  $\pm$  SD; One-way ANOVA). \* $P < 0.05$ , \*\* $P < 0.01$ , \*\*\* $P < 0.001$ , ns: no significance.

secretion was reversed by the miR-29a-3p antagomir (Supporting Information Fig. S7). Previous work has shown that chemotherapy drugs, including cisplatin and paclitaxel, accumulate in exosomes<sup>28,29</sup>. To exclude the influence of exosomal cisplatin on the modification of collagen from fibroblasts, we stimulated fibroblasts with cisplatin (5  $\mu\text{mol/L}$ , 24 h) directly. Interestingly, cisplatin treatment did not down-regulate the expression of collagen I in lung fibroblasts (Supporting Information Fig. S8A). In addition, cisplatin treatment did not up-regulate the level of miR-29a-3p in lung fibroblasts, which suggested the origin of miR-29a-3p is mainly derived from tumor cells during chemotherapy *in vivo* (Fig. S8B). These results indicate that increased miR-29a-3p load in CPT-Exo plays a key role in down-regulating collagen I expression in lung fibroblasts.

### 3.3. miR-29a-3p loaded into CPT-Exo regressed lung tumor cell metastasis *in vitro* and *in vivo*

Collagens are well-known ECM components that can influence tumor cell behavior in the multiple processes of tumor cell metastasis, including tumor cell adhesion, migration, invasion, and proliferation<sup>6,8</sup>. To investigate if miR-29a-3p delivery could influence tumor cell adhesion by targeting collagen I, we first transfected primary lung fibroblasts with the miR-29a-3p mimic and then stimulated LLC cells with its conditional culture medium. We found that the attachment of LLC-mCherry cells in the miR-29a-3p mimic pre-transfected fibroblasts was significantly reduced (Supporting Information Fig. S9A). Additionally, supernatant collected from miR-29a-3p transfected fibroblasts had a

weaker effect in inducing LLC colony formation, invasion, and differentiation (Fig. S9B–S9D). On the contrary, the miR-29a-3p antagomir reversed the CPT-Exo down-regulated LLC adhesion, colony formation, invasion, and proliferation (Fig. S9). Therefore, CPT-Exo plays a major role in alleviating the positive impact of collagen I expression on inducing tumor cell metastasis in the lung *in vitro* by delivering miR-29a-3p.

We next wanted to investigate if the enriched miR-29a-3p in CPT-Exo could influence lung tumor metastasis in the lung. For this purpose, we first pretreated mice with exosomes three times in nine days, followed by intravenous injection of LLC cells (Fig. 3A). Three weeks later, we observed a significant tumor cell metastasis in the lung of the LLC-Exo group (Fig. 3B). Interestingly, the number of metastatic lung tumors in CPT-Exo pretreated mice was significantly decreased, and the tumor area was diminished (Fig. 3C). These results suggest that CPT-Exo can suppress circulating lung tumor cell metastasis in the lung. In addition, CPT-Exo treatment in tumor burdened lungs showed reduced collagen I staining in metastatic sites and tumor-free lung tissue (Fig. 3D and E). We thus speculate that reduced collagen I in the lung may play a role in reducing lung tumor metastasis.

### 3.4. Liposomal nanovesicle-based miR-29a-3p delivery abrogates metastatic colonization of lung tissue

We have shown that miR-29a-3p loaded into CPT-Exo plays a major role in down-regulating collagen I expression in fibroblasts and thus potentially affects the key steps of tumor cell metastasis *in vitro*. However, unknown factors in CPT-Exo may present major

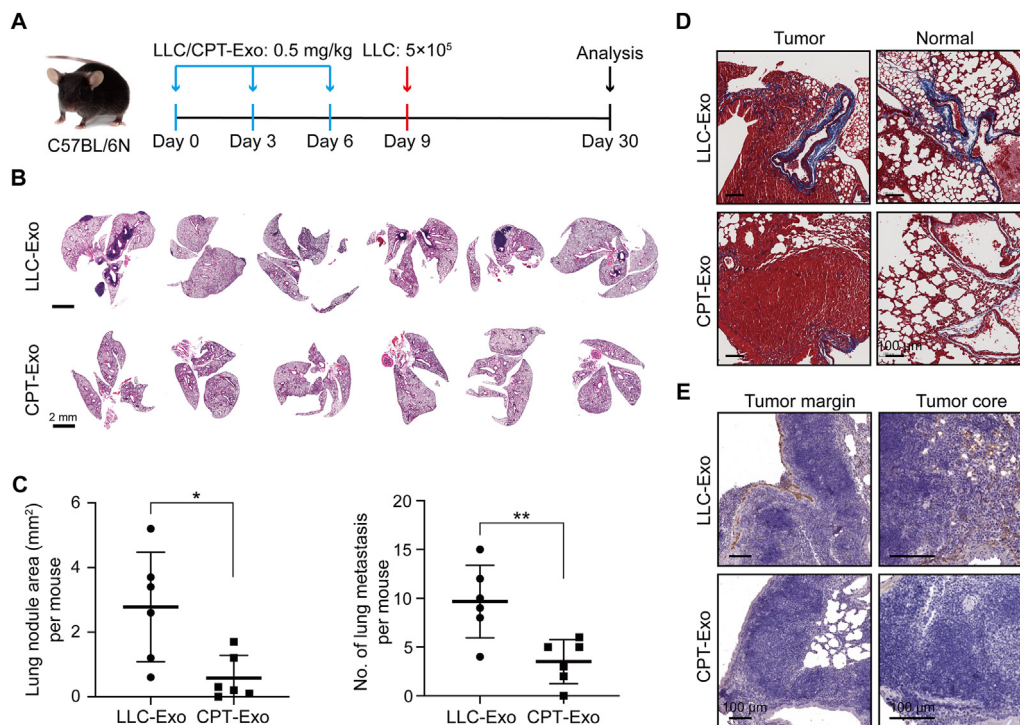


**Figure 3** CPT-Exo regressed lung tumor cell colonization in the lungs. (A) Schematic illustrating the exosome treatments for tumor colonization experiments. (B) Lung HE images from mice used in the experiment shown in A. Scale bar = 2 mm. (C) Quantification of the total area (left) and numbers (right) of mice lung metastatic nodules in two groups ( $n = 6$  per group; mean  $\pm$  SD; Welch's *t*-test). \* $P < 0.05$ , \*\* $P < 0.01$ . (D) Masson staining was used to identify the total collagen expression level in LLC-injected CPT-Exo or LLC-Exo pretreated lungs. Representative tumor or tumor-free areas are shown. (E) IHC staining to monitor collagen I levels in the tumor margin and tumor core from the two groups. Scale bar = 100  $\mu\text{m}$ .

challenges for future clinical studies. To improve the efficiency of delivery, we designed a liposome-packed miR-29a-3p system, miR-29a-3p-LPX. Characterization of miR-29a-3p-LPX showed that it has a similar size to exosomes ( $131.6 \pm 8.1$  nm, Fig. 4A and B). Moreover, the colloidal solution of miR-29a-3p-LPX was colorless, transparent, and had a clear Tyndall effect compared with water, indicating the existence of abundant nanoparticles that were completely dispersed in aqueous media (Fig. 4C). The biocompatibility of miR-29a-3p-LPX was evaluated by its hemolytic activity, and no hemolysis was observed (Fig. 4D). Based on a previous publication<sup>19</sup>, adjusting the charge/mass ratio of liposome to miR-29a-3p to 4:1 allowed us to specifically locate miR-29a-3p to lung tissue (Fig. 4E). We also established a miR-

29a-3p-LPX pretreated mouse model (Fig. 4F). After intravenously injecting LLC-EGFP-Luc cells, we observed the tumor cell number at different time points and found that the number of CTCs at 72 h were similar (Fig. 4G), although the number of tumor cells in the miR-29a-3p-LPX pretreated groups was significantly lower (Fig. 4H). This result suggests that down-regulation of collagen I expression mediated by miR-29a-3p contributes to tumor cell seeding in the lung.

Next, we investigated the effect of liposomal-based nanovesicle-delivery on lung tumor cell metastasis (Fig. 5A). We observed a significant reduction in metastatic sites in the miR-29a-3p-LPX group after 21 days (Fig. 5B–E). These results suggest that CPT-Exo and miR-29a-3p-LPX pretreatment could suppress

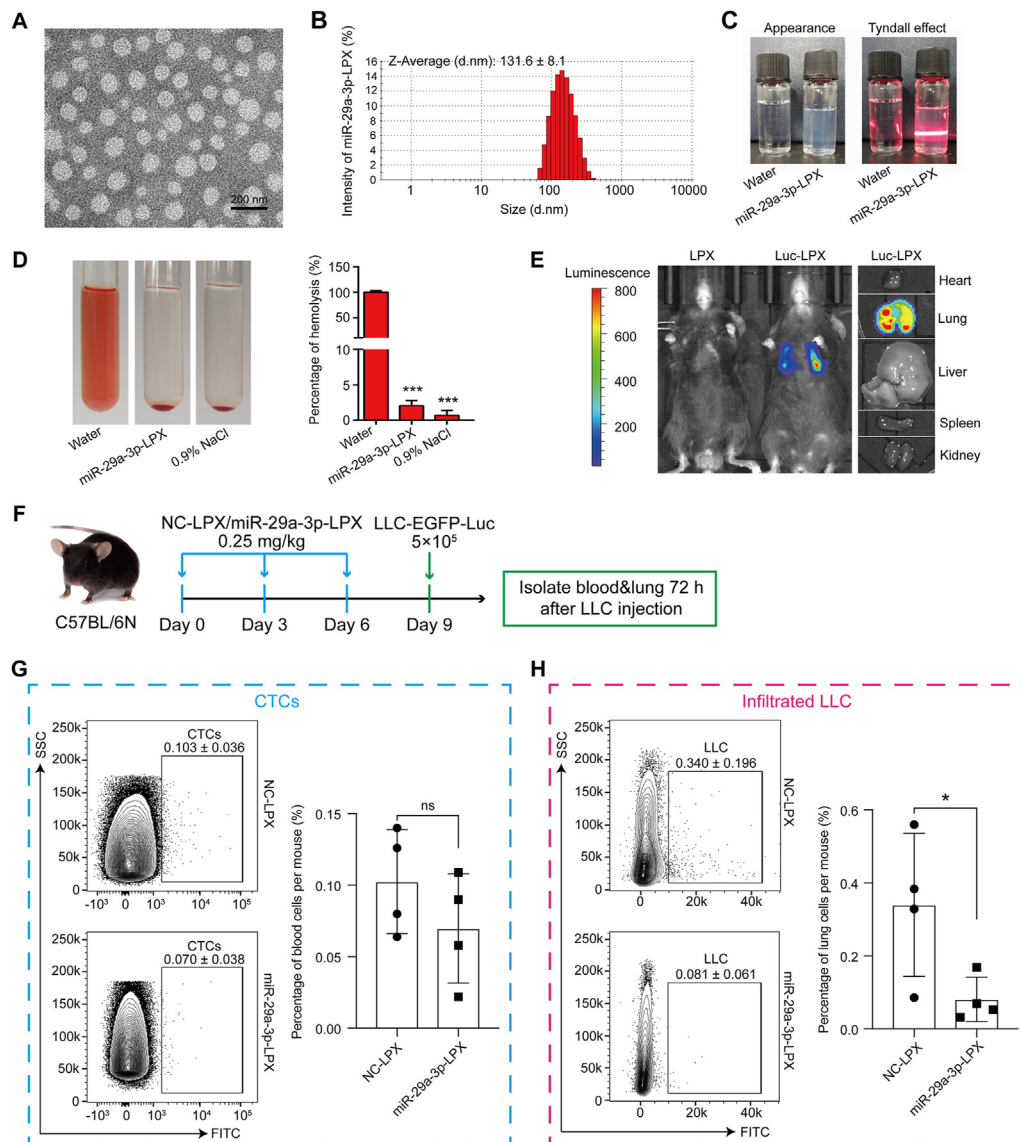


**Figure 4** Characterization and lung-targeted delivery of miR-29a-3p-LPX. (A) Representative TEM image of miR-29a-3p-LPX. Scale bar = 200 nm. (B) The particle size distribution histogram of miR-29a-3p-LPX obtained from Zetasizer analysis on a Malvern Zetasizer instrument. (C) Appearance (left) and Tyndall effect (right) of miR-29a-3p-LPX. (D) Hemolytic analysis of miR-29a-3p-LPX. (E) Bioluminescence imaging of mice injected with LPX or Luc-LPX. (F) Schematic illustrating miR-29a-3p-LPX and NC-LPX treated tumor colonization assays. Flow cytometry analysis of the CTCs frequency in the peripheral blood (G) and the infiltrated LLC cells frequency in lungs (H) of mice from the experiment shown in F collected 72 h after LLC-EGFP-Luc injection ( $n = 4$  per group; mean  $\pm$  SD; Welch's  $t$ -test). \* $P < 0.05$ , \*\*\* $P < 0.001$ , ns: no significance.

tumor cell metastasis in the lung. To examine if miR-29a-3p has the potential to inhibit tumor cell metastasis when the primary tumor cells are *in situ*, we seeded LLC cells in the lung *via* the bloodstream and then administered miR-29a-3p-LPX three times (Fig. 6A). Similarly, miR-29a-3p treatment reduced lung tumor metastasis (Fig. 6B–E). In addition, we compared the therapeutic effect of CPT-Exo and miR-29a-3p-LPX in our tumor model. However, we did not observe a significant difference in the amount of metastatic colonization and tumor area (Supporting Information Fig. S10).

### 3.5. miR-29a-3p positively correlates with the outcome of lung cancer patients

Having shown that miR-29a-3p delivery could reduce tumor cell metastasis in the lung, we wanted to study the predictive potential of miR-29a-3p on lung cancer prognosis. We first compared the expression of collagen I with patient survival rate using public lung cancer datasets<sup>30</sup>. We found that lung-adenocarcinoma patients with high collagen I expression had a significantly lower survival. In addition, we noticed that lung-adenocarcinoma patients with high levels of miR-29a expression had better survival rates (Fig. 7A). These results indicate that miR-29a should be further investigated as a biomarker for predicting the prognosis of lung adenocarcinoma patients. To study the correlation between miR-29a and collagen I expression in lung adenocarcinoma

patients, we analyzed the expression of miR-29a-3p and *COL1A1* in a cohort of lung adenocarcinoma patients (Fig. 7B–E). We found miR-29a-3p to be highly expressed on para-tumor tissue (Fig. 7D). Compared with low-grade lung tumor patients, high-grade tumor patients have lower levels of miR-29a-3p expression (Fig. 7E). Importantly, a comparison of miR-29a-3p expression with *COL1A1* expression revealed a significant negative correlation, which further suggests that miR-29a-3p may exert its tumor suppressive function by directly targeting collagen I expression (Fig. 7F). Moreover, we detected the circulating exosomal miR-29a-3p in lung cancer patients. Compared with healthy donors, the level of miR-29a-3p in lung cancer patients was significantly lower (Fig. 7G); among lung cancer patients, patients with higher levels of miR-29a-3p had better survival rates (Fig. 7H). These data suggest that reduced miR-29a-3p levels are a potential predictor of patients' outcomes in lung cancer.

## 4. Discussion

Tumor metastasis is the primary cause of tumor-related deaths. Due to a lack of specificity and low bioavailability affecting therapeutic efficacy, current tumor treatments still represent a formidable challenge. Increasing evidence indicates that nanovesicles can overcome various biological barriers and localize at tumor sites<sup>31</sup>. In this study, we identified exosomes released from lung tumor cells after cisplatin stimulation as natural carriers of

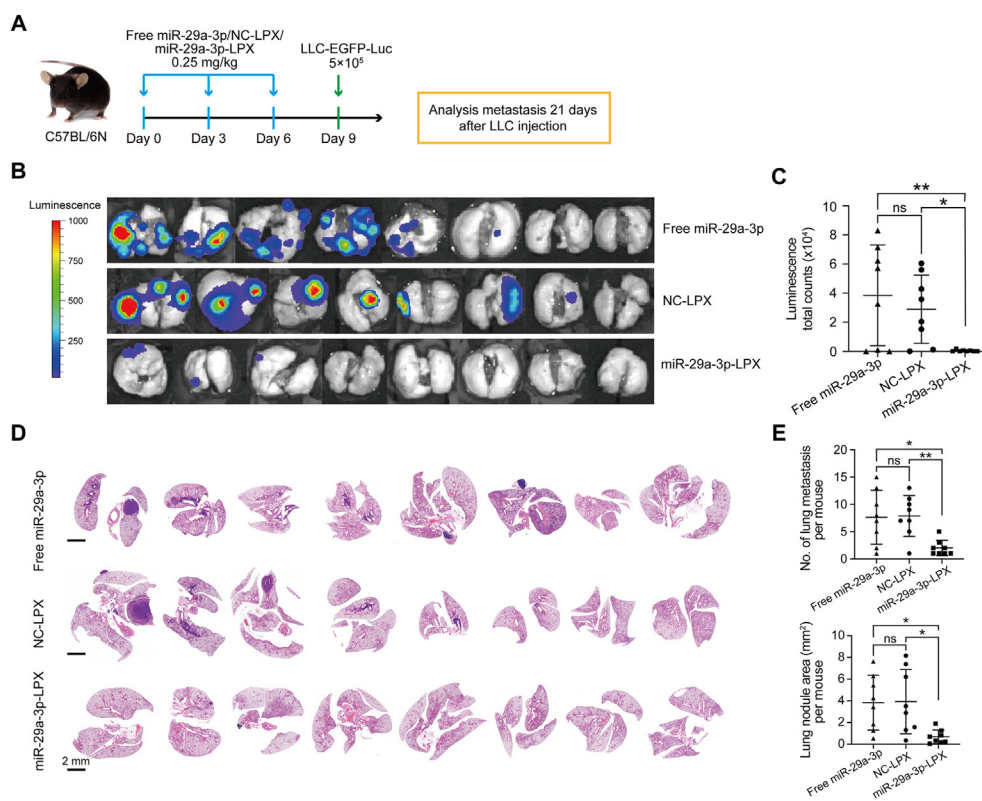


**Figure 5** miR-29a-3p delivery *in vivo* abrogates metastatic colonization in the lung. (A) Schematic illustrating miR-29a-3p-LPX, NC-LPX or free miR-29a-3p treated tumor colonization assays. (B) Bioluminescence images of lung metastatic colonization from miR-29a-3p-LPX, NC-LPX or free miR-29a-3p treated mice 21 days after tail-vein injection of LLC-EGFP-Luc cells. (C) Quantifications of the bioluminescence are shown ( $n = 8$  per group). (D) HE images of the lung sections of mice from the experiment shown in A. Scale bar = 2 mm. (E) Quantification of the numbers (top) and total area (bottom) of mice lung metastatic nodules in different groups ( $n = 8$  per group). Data in C and E are mean  $\pm$  SD; Welch's *t*-test. \* $P < 0.05$ , \*\* $P < 0.01$ .

biological cargoes that can be enriched in the lung. The enhanced levels of miR-29a-3p in CPT-Exo show effective therapeutic capacity by suppressing the production of collagen I from lung fibroblasts. Moreover, liposomal packaged miR-29a-3p delivery was identified as a potential therapeutic method for preventing tumor cell metastasis. The anti-tumor metastasis effect of delivering these nanovesicles opens new avenues for therapeutic intervention in lung tumor metastasis and deepens our understanding of the mechanistic relevance of miRNAs contained in exosomes.

Tumor-derived exosomes participate in tumor progression and metastasis by communicating with the tumor microenvironment are vital to establishing the pre-metastatic niche (PMN)<sup>18,32–34</sup>. Our previous study identified that lung tumor cell-derived exosomes facilitate lung tumor cell colonization in the lung by activating NF- $\kappa$ B signaling of lung fibroblasts<sup>25</sup>. Similarly, the uptake of breast cancer-derived exosomes by lung fibroblasts promoted their activation and fibronectin secretion, thus contributing to PMN formation and lung metastasis<sup>35</sup>. Although the tumor-promoting function of these primary tumor cell-derived exosomes has been indicated, surprisingly, our study found that the enhanced miR-29a-3p loaded in CPT-Exo had significant tumor metastatic inhibition. It is speculated that other factors loaded in CPT-Exo may present distinct tumor-promoting or inhibiting functions, which need future investigation.

Cisplatin is the most frequently used chemotherapy drug for lung cancer treatment, and interestingly, our results showed that CPT-Exo reduced lung tumor cell metastasis in the lung. We speculate that chemotherapy induces the release of tumor EVs and exosomes, which may inhibit tumor metastatic function. In this study, we identified up-regulation of miR-29a-3p in CPT-Exo,

which inhibited lung tumor cell metastasis by decreasing the expression of collagen I in lung fibroblasts. Although a minimal amount of cisplatin loaded into CPT-Exo could influence tumor growth, we did not observe a reduced number of LLC cells circulating at 72 h after CPT-Exo pretreatment and LLC injection. We thus speculate that the up-regulated miR-29a-3p in CPT-Exo elicits collagen I down-regulation and may play a key role in inhibiting lung tumor cell metastasis. Future studies should also consider the influence of chemotherapy drugs on exosome release in fibroblasts, immune cells, and other tumor stromal cells because tumor and stromal cells continuously receive stimulation by chemotherapy.

Fibroblasts are the major cell types in the lung that can produce high levels of collagens. Our previous study indicated that primary lung tumor-derived exosomes could be uptaken by lung fibroblasts<sup>25</sup>. It is, therefore, suggested that exosomal nanovesicles are ideal carriers for targeting fibroblasts. Although this study indicated that LLC cells contained higher amounts of miR-29a-3p, our initial study proved that primary lung tumor cell-derived exosomes facilitated CTCs colonization in the lung<sup>25</sup>. Chemotherapy not only increased the number but also altered the cargo loads of tumor EVs<sup>36</sup>. Here, we identified that cisplatin exposure led to increased loading of miR-29a-3p into CPT-Exo, which abrogated the metastatic capacity of circulating lung tumor cells in the lung by inhibiting collagen I expression in lung fibroblasts. We observed fewer lung metastatic sites in CPT-Exo pretreated mice; this indicates that the modification of the cargo loaded into CPT-Exo reversed the tumor-promoting function of primary LLC exosomes, in which enhanced miR-29a-3p may play a key role. This also suggested the therapeutic potential of miR-29a-3p-enriched exosomal nanovesicles for tumor metastasis in the lung.

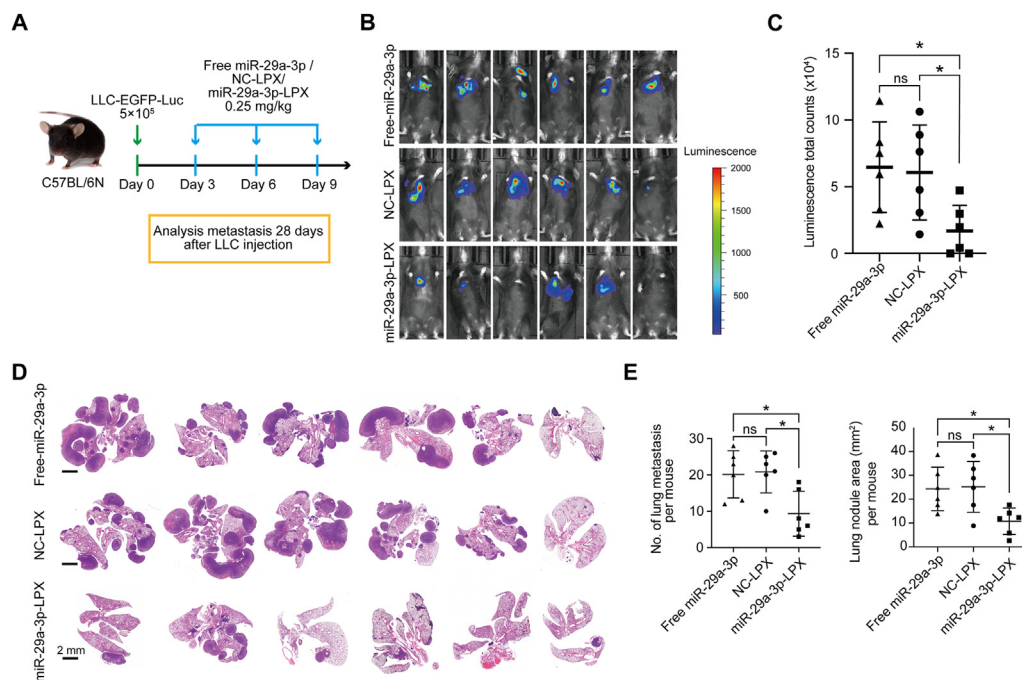


**Figure 6** miR-29a-3p-LPX treatment inhibits the growth of metastatic tumors. (A) Schematic illustrating the animal experiments involving miR-29a-3p-LPX, NC-LPX or free miR-29a-3p treatment after LLC-EGFP-Luc tail-vein injection. (B) Bioluminescence images of lung metastatic tumor growth in mice from the experiment shown in A. (C) Quantifications of the bioluminescence are shown ( $n = 6$  per group). (D) HE images of the lung sections of mice from the experiment shown in A. Scale bar = 2 mm. (E) Quantification of the numbers (left) and total area (right) of mice lung metastatic nodules in different groups ( $n = 6$  per group). Data in C and E are mean  $\pm$  SD; Welch's  $t$ -test. \* $P < 0.05$ .

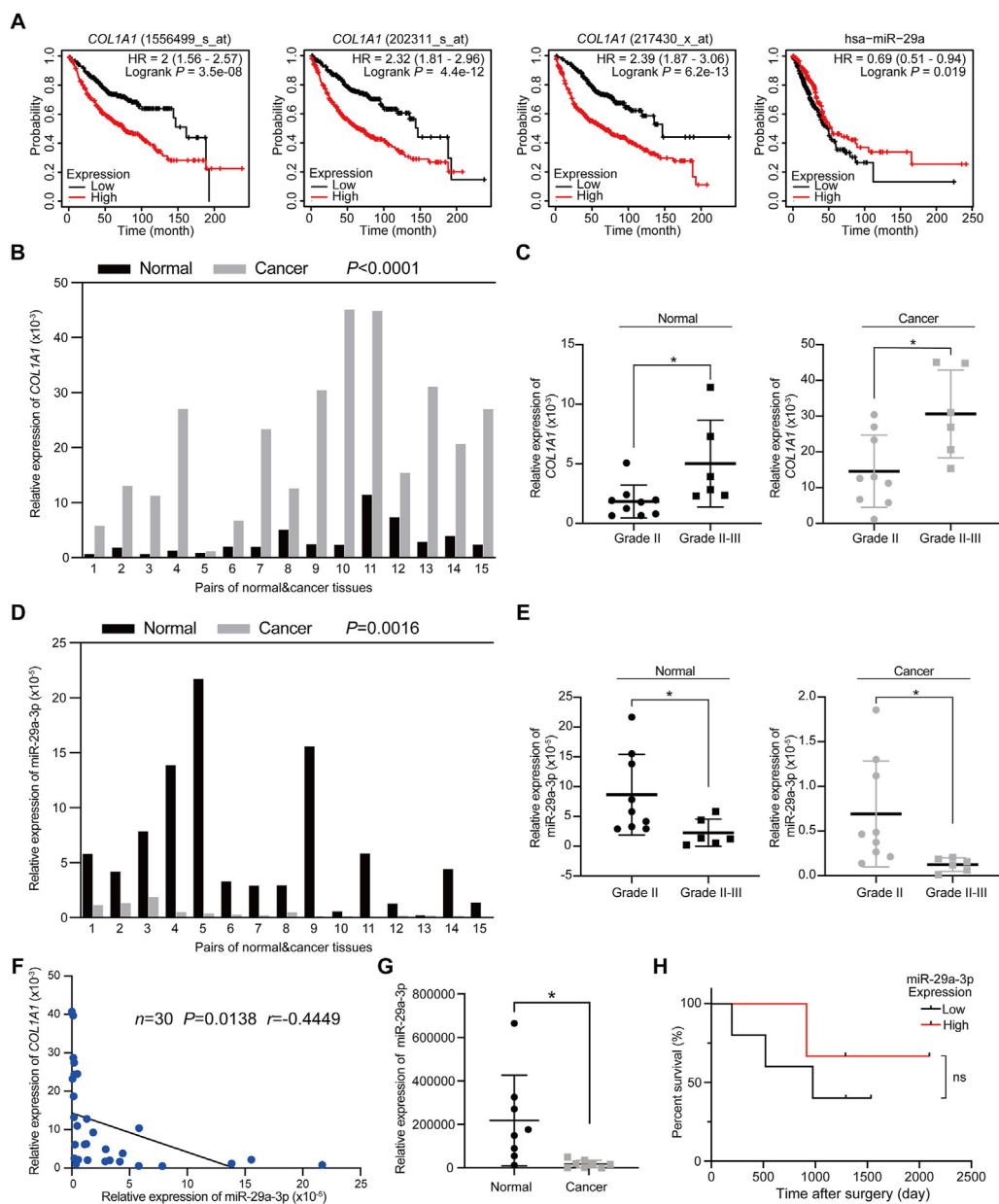


**Figure 7** Correlation between miR-29a-3p expression and collagen I in human lung cancer patients. (A) Kaplan–Meier survival analysis of *COL1A1* and miR-29a-3p expression in lung cancer patients. (B) Relative *COL1A1* expression in 15 pairs of lung adenocarcinoma tissues and adjacent normal tissues, determined by qRT-PCR ( $n = 15$ ; two-tailed, paired  $t$ -test). (C) Comparison of *COL1A1* levels of normal tissues (left panel) and lung cancer tissues (right panel) in different lung cancer grades (mean  $\pm$  SD; Grade II,  $n = 9$ ; Grade II-III,  $n = 6$ ; Welch's  $t$ -test.  $*P < 0.05$ ). (D) Relative miR-29a-3p expression levels in 15 pairs of lung adenocarcinoma tissues and adjacent normal tissues, determined by qRT-PCR ( $n = 15$ ; two-tailed, paired  $t$ -test). (E) Comparison of the relative miR-29a-3p levels of normal tissues (left panel) and lung cancer tissues (right panel) in different lung cancer grades (mean  $\pm$  SD; Grade II,  $n = 9$ ; Grade II-III,  $n = 6$ ; Welch's  $t$ -test.  $*P < 0.05$ ). (F) Correlation between *COL1A1* and hsa-miR-29a-3p levels. The Pearson correlation coefficient is indicated ( $n = 30$ ,  $P = 0.0138$ ,  $r = -0.4449$ ). (G) Relative miR-29a-3p expression in circulating exosomes ( $n = 8$ ; mean  $\pm$  SD; Welch's  $t$ -test). (H) Correlation of circulating miR-29a-3p expression with overall survival in lung adenocarcinoma patients (low expression,  $n = 5$ ; high expression,  $n = 3$ ; ns: no significance).

miRNAs play important roles in tumor progression<sup>37</sup> through tumor suppressor inactivation or pathways such as MAPK and AKT<sup>38</sup> or p53<sup>39</sup>. miRNAs are promising therapeutic targets<sup>37</sup>, although miRNA antagonists or mimics are quickly degraded and cleared, and tissue-specific delivery is challenging<sup>40</sup>. In this study, we designed a liposome packaged miRNA system RNA-lipoplex, which could protect miRNA from degradation and increase the stability of miRNAs in circulation<sup>19</sup>. In addition, by

adjusting the charge ratio of DOTAP/cholesterol to miRNAs to 4:1, we showed that the miR-29a-3p mimic could be specifically delivered to the lung. The increased miR-29a-3p enrichment in the lung efficiently decreased lung tumor cell colonization. Although it has been confirmed that the miRNAs can be specifically sent to the lung and spleen by modifying their ratio with liposomes, the underlying mechanisms are still under investigation.

miR-29 has been recognized as a critical miRNA in various cancers, regulating multiple oncogenic processes<sup>41</sup>. miR-29 exhibits strong anti-fibrotic activity by negatively regulating of ECM proteins, including collagens and fibrillin<sup>26,42</sup>. Our data confirmed miR-29a-3p alone or contained in CPT-Exo could significantly down-regulate collagen I expression in lung fibroblasts. Some studies have indicated a tumor-promoting function of miR-29, but the majority of publications have demonstrated its tumor suppressor properties by inhibiting various tumor development-related targets, such as proliferation, angiogenesis, or epithelial–mesenchymal transition<sup>41</sup>. Our clinical data indicated that lung cancer patients with high miR-29a-3p expression achieved better survival outcomes than those with low miR-29a-3p expression, suggesting a potential prognostic value and therapeutic target for miR-29a-3p in lung cancers. Interestingly, RNA-LPX-based miR-29a-3p delivery significantly reduced metastatic sites in the lung, indicating interesting avenues of research that may lead to the development of therapeutic interventions aimed to enrich miR-29a-3p accumulation in the lung.

Comparing the two delivery systems we used in this study, the exosomal nanovesicles showed excellent biological compatibility, superior to liposomal nanovesicles, and particularly small size, thus acting as natural carriers for miR-29a-3p transfer. However, unknown factors, including other miRNAs and proteins in the exosomes, may cause uncertain side-effects during tumor treatment. On the contrary, liposomal nanovesicles have clear content and can be sent to specific organs but show low biological compatibility and are often detected by immune cells, so their biological safety in preclinical studies needs to be reevaluated. Future studies should take advantage of the features of these two nanovesicles and exploit specific miRNA-loading exosomal-based nanovesicles for the delivery of therapeutic drugs and nucleic acids.

## 5. Conclusions

In summary, our study demonstrates the inhibition of lung tumor metastasis by the transmission of miR-29a-3p in the manner of tumor exosomes or liposomal-based nanovesicles, thereby decreasing collagen I expression in lung fibroblasts and restraining metastasis by undermining the establishment of a viable PMN.

## Acknowledgments

We thank Dr. Jessica Tamanini from Insight Editing London for critical reading of the manuscript. This work was supported by the National Natural Science Foundation of China (Grant Nos. 81630068, 31670881, and 81901466) and China Postdoctoral Science Foundation (Grant No. 2020TQ0282).

## Author contributions

Zhihai Qin, Ming Wang and Fazhan Wang designed the research. Yan Yan carried out the experiments and performed data analysis. Cancan Du, Xixi Duan, Xiaohan Yao, Jiajia Wan, Ziming Jiang, Zhongyu Qin, Wenqing Li, Longze Pan and Zhuoyu Gu participated part of the experiments. Fazhan Wang provided experimental drugs and quality control. Ming Wang and Yan Yan wrote the manuscript. Zhihai Qin revised the manuscript. All of the authors have read and approved the final manuscript.

## Conflicts of interest

The authors have no conflicts of interest to declare.

## Appendix A Supporting information

Supporting data to this article can be found online at <https://doi.org/10.1016/j.apsb.2021.08.011>.

## References

1. Fares J, Fares MY, Khachfe HH, Salhab HA, Fares Y. Molecular principles of metastasis: a hallmark of cancer revisited. *Signal Transduct Target Ther* 2020;**5**:28.
2. Hanahan D, Weinberg RA. The hallmarks of cancer. *Cell* 2000;**100**:57–70.
3. Lambert AW, Pattabiraman DR, Weinberg RA. Emerging biological principles of metastasis. *Cell* 2017;**168**:670–91.
4. Stella GM, Kolling S, Benvenuti S, Bortolotto C. Lung-seeking metastases. *Cancers (Basel)* 2019;**11**:1010.
5. Altorki NK, Markowitz GJ, Gao D, Port JL, Saxena A, Stiles B, et al. The lung microenvironment: an important regulator of tumour growth and metastasis. *Nat Rev Cancer* 2019;**19**:9–31.
6. Nissen NI, Karsdal M, Willumsen N. Collagens and cancer associated fibroblasts in the reactive stroma and its relation to cancer biology. *J Exp Clin Cancer Res* 2019;**38**:115.
7. Barcus CE, O'Leary KA, Brockman JL, Rugowski DE, Liu Y, Garcia N, et al. Elevated collagen-I augments tumor progressive signals, intravasation and metastasis of prolactin-induced estrogen receptor alpha positive mammary tumor cells. *Breast Cancer Res* 2017;**19**:9.
8. Winkler J, Abisoye-Ogunniyan A, Metcalf KJ, Werb Z. Concepts of extracellular matrix remodelling in tumour progression and metastasis. *Nat Commun* 2020;**11**:5120.
9. Xiong G, Chen J, Zhang G, Wang S, Kawasaki K, Zhu J, et al. Hsp47 promotes cancer metastasis by enhancing collagen-dependent cancer cell–platelet interaction. *Proc Natl Acad Sci U S A* 2020;**117**:3748–58.
10. Lee YC, Kurtova AV, Xiao J, Nikolos F, Hayashi K, Tramel Z, et al. Collagen-rich airway smooth muscle cells are a metastatic niche for tumor colonization in the lung. *Nat Commun* 2019;**10**:2131.
11. Fang M, Yuan J, Peng C, Li Y. Collagen as a double-edged sword in tumor progression. *Tumour Biol* 2014;**35**:2871–82.
12. Wang JK, Wang Z, Li G. MicroRNA-125 in immunity and cancer. *Cancer Lett* 2019;**454**:134–45.
13. Xu S, Xu H, Wang W, Li S, Li H, Li T, et al. The role of collagen in cancer: from bench to bedside. *J Transl Med* 2019;**17**:309.
14. Jafarnejad-Farsangi S, Gharibdoost F, Farazmand A, Kavosi H, Jamshidi A, Karimizadeh E, et al. MicroRNA-21 and microRNA-29a modulate the expression of collagen in dermal fibroblasts of patients with systemic sclerosis. *Autoimmunity* 2019;**52**:108–16.
15. Yu PN, Yan MD, Lai HC, Huang RL, Chou YC, Lin WC, et al. Downregulation of miR-29 contributes to cisplatin resistance of ovarian cancer cells. *Int J Cancer* 2014;**134**:542–51.
16. Kalluri R, LeBleu VS. The biology function and biomedical applications of exosomes. *Science* 2020;**367**:eaa6977.
17. Arrighetti N, Corbo C, Evangelopoulos M, Pastò A, Zuco V, Tasciotti E. Exosome-like nanovectors for drug delivery in cancer. *Curr Med Chem* 2019;**26**:6132–48.
18. Wortzel I, Dror S, Kenific CM, Lyden D. Exosome-mediated metastasis: communication from a distance. *Dev Cell* 2019;**49**:347–60.
19. Kranz LM, Diken M, Haas H, Kreiter S, Loquai C, Reuter KC, et al. Systemic RNA delivery to dendritic cells exploits antiviral defence for cancer immunotherapy. *Nature* 2016;**534**:396–401.
20. Keerthisingam CB, Jenkins RG, Harrison NK, Hernandez-Rodríguez NA, Booth H, Laurent GJ, et al. Cyclooxygenase-2 deficiency results in a loss of the anti-proliferative response to

- transforming growth factor-beta in human fibrotic lung fibroblasts and promotes bleomycin-induced pulmonary fibrosis in mice. *Am J Pathol* 2001;**158**:1411–22.
21. Putz U, Mah S, Goh CP, Low LH, Howitt J, Tan SS. PTEN secretion in exosomes. *Methods* 2015;**77–78**:157–63.
  22. Vinci M, Box C, Eccles SA. Three-dimensional (3D) tumor spheroid invasion assay. *J Vis Exp* 2015;**0**:e52686.
  23. Wang F, Xiao W, Elbahnasawy MA, Bao X, Zheng Q, Gong L, et al. Optimization of the linker length of mannose-cholesterol conjugates for enhanced mRNA delivery to dendritic cells by liposomes. *Front Pharmacol* 2018;**9**:980.
  24. Chen Z, Peng Y, Xie X, Feng Y, Li T, Li S, et al. Dendrimer-functionalized superparamagnetic nanobeacons for real-time detection and depletion of *HSP90 $\alpha$*  mRNA and MR Imaging. *Theranostics* 2019;**9**: 5784–96.
  25. Du C, Duan X, Yao X, Wan J, Cheng Y, Wang Y, et al. Tumor-derived exosomal miR-3473b promotes lung tumour cell intrapulmonary colonization by activating the nuclear factor- $\kappa$ B of local fibroblasts. *J Cell Mol Med* 2020;**24**:7802–13.
  26. Cushing L, Kuang P, Lü J. The role of miR-29 in pulmonary fibrosis. *Biochem Cell Biol* 2015;**93**:109–18.
  27. Maurer B, Stanczyk J, Jüngel A, Akhmetshina A, Trenkmann M, Brock M, et al. MicroRNA-29, a key regulator of collagen expression in systemic sclerosis. *Arthritis Rheum* 2010;**62**:1733–43.
  28. Safaei R, Larson BJ, Cheng TC, Gibson MA, Otani S, Naerdemann W, et al. Abnormal lysosomal trafficking and enhanced exosomal export of cisplatin in drug-resistant human ovarian carcinoma cells. *Mol Cancer Ther* 2005;**4**:1595–604.
  29. Pascucci L, Coccè V, Bonomi A, Ami D, Ceccarelli P, Ciusani E, et al. Paclitaxel is incorporated by mesenchymal stromal cells and released in exosomes that inhibit *in vitro* tumor growth: a new approach for drug delivery. *J Control Release* 2014;**192**:262–70.
  30. Gyórfy B, Surowiak P, Budczies J, Lánckzy A. Online survival analysis software to assess the prognostic value of biomarkers using transcriptomic data in non-small-cell lung cancer. *PLoS One* 2013;**8**: e82241.
  31. Valcourt DM, Harris J, Riley RS, Dang M, Wang J, Day ES. Advances in targeted nanotherapeutics: from bioconjugation to biomimicry. *Nano Res* 2018;**11**:4999–5016.
  32. Tkach M, Thery C. Communication by extracellular vesicles: where we are and where we need to go. *Cell* 2016;**164**:1226–32.
  33. Hoshino A, Costa-Silva B, Shen TL, Rodrigues G, Hashimoto A, Tesic Mark M, et al. Tumour exosome integrins determine organotropic metastasis. *Nature* 2015;**527**:329–35.
  34. Lobb RJ, Lima LG, Möller A. Exosomes: key mediators of metastasis and pre-metastatic niche formation. *Semin Cell Dev Biol* 2017;**67**: 3–10.
  35. Liu Y, Gu Y, Han Y, Zhang Q, Jiang Z, Zhang X, et al. Tumor exosomal RNAs promote lung pre-metastatic niche formation by activating alveolar epithelial TLR3 to recruit neutrophils. *Cancer Cell* 2016;**30**:243–56.
  36. Ab Razak NS, Ab Mutalib NS, Mohtar MA, Abu N. Impact of chemotherapy on extracellular vesicles: understanding the chemo-EVs. *Front Oncol* 2019;**9**:1113.
  37. Zhang L, Liao Y, Tang L. MicroRNA-34 family: a potential tumor suppressor and therapeutic candidate in cancer. *J Exp Clin Cancer Res* 2019;**38**:53.
  38. Bautista-Sánchez D, Arriaga-Canon C, Pedroza-Torres A, De La Rosa-Velázquez IA, González-Barrios R, Contreras-Espinosa L, et al. The promising role of miR-21 as a cancer biomarker and its importance in RNA-based therapeutics. *Mol Ther Nucleic Acids* 2020;**20**: 409–20.
  39. Navarro F, Lieberman J. miR-34 and p53: new insights into a complex functional relationship. *PLoS One* 2015;**10**:e0132767.
  40. Chen Y, Gao DY, Huang L. *In vivo* delivery of miRNAs for cancer therapy: challenges and strategies. *Adv Drug Deliv Rev* 2015;**81**:128–41.
  41. Kwon JJ, Factora TD, Dey S, Kota J. A Systematic review of miR-29 in cancer. *Mol Ther Oncolytics* 2019;**12**:173–94.
  42. van Rooij E, Sutherland LB, Thatcher JE, DiMaio JM, Naseem RH, Marshall WS, et al. Dysregulation of microRNAs after myocardial infarction reveals a role of miR-29 in cardiac fibrosis. *Proc Natl Acad Sci U S A* 2008;**105**:13027–32.